31st International Conference Nuclear Energy for New Europe
NENE 2022
September 12-15
PORTOROŽ
SLOVENIA

Importance of Physics-aware Use of Area Validation Metric for LES Methanol Pool Fire Simulation Data

Jared Kirsch[1,2]

[1]University of New Mexico, NM, USA
[2]Sandia National Laboratories, NM, USA
jkirschbusiness@gmail.com

Nima Fathi[1,3*]

[1]University of New Mexico, NM, USA
[3]Texas A&M University, TX, USA
nfathi@tamu.edu

ABSTRACT

A 0.3-m diameter methanol pool fire was modelled using Sandia National Laboratories SIERRA/Fuego turbulent reacting flow code. The turbulence model used was the Large Eddy Simulation (LES) turbulence model, and combustion modelling utilized a strained laminar flamelet library approach. Transient analysis of simulation results was conducted using the area validation metric (AVM) with multiple time intervals chosen for the data. Conclusions were drawn regarding appropriate time interval sizes for use of such a metric in the quantification of uncertainty in simulation results.

1 INTRODUCTION

Validation analysis of simulation data from transient physics scenarios often involves temporal averaging, and/or analysis of distributions of data over time. Such analysis requires understanding of the physical scenario being modelled, and what time ranges are appropriate to use for statistical analysis and temporal averaging. In addition, a robust validation metric should be applied in order to achieve objective, useful, validation. The AVM is a validation metric which provides objective comparisons of simulation results to experimental data, where one or both are in the form of distributions. One of the earliest descriptions of such a metric was from Ferson et al. [1], and the AVM was popularized in large part by Oberkampf and Roy [2]. Specifically, the modified area validation metric, with separate quantification of positive and negative differences between simulation and experiment, is used in this study, and this metric will simply be referred to as the area validation metric.

As part of the validation effort for the SIERRA/Fuego code, specific validation cases are used due to the fact that experiments of such cases are conducted for validation purposes specifically, and the associated data quality, descriptions of necessary parameters for reproductive simulations, and measurement reports are typically commensurate with that fact. Another advantage of using such a validation case is that a community of researchers typically uses the case, and thus other validation efforts can be used to inform future attempts. Such was the case with the methanol pool fire simulated in this study. The 30-cm diameter methanol pool fire is a specific validation case of the International Association for Fire Safety Science (IAFSS) Working Group on Measurement and Computation of Fire Phenomena (MaCFP Working Group). This moderate-scale, non-sooting pool fire has been well characterized experimentally, with several detailed studies being reported in [3-10]. Weckman conducted an early and foundational study on this case, and provided a dataset containing mean and RMS values of velocity and temperature, as well as, length scales, turbulence intensity, and correlations.

*Corresponding author

Several National Institute of Science and Technology (NIST) experimental studies have also been conducted on this case, and the study of Hamins et al. [11] includes a dataset for radiative heat flux.

In this study, the AVM is used to compute areas which are related to uncertainties on the numerical results. This is done for a representative location for temperature, axial velocity, and heat flux. For each of these quantities of interest (QOIs), several time intervals are used to draw data from the simulation results, and the effect of the time interval length is examined. It is seen that a sufficiently long time interval is necessary to effectively use a metric such as the AVM, and that an understanding of appropriate time interval sizes is related to an understanding of the physical phenomena involved in the simulated scenario.

2 SIMULATION DETAILS

The code used to perform the simulations analyzed in this study is Sandia National Laboratories' SIERRA Fuego code. SIERRA Fuego is a low-Mach, turbulent reacting flow code, which is the primary simulation code in the ASC fire environment simulation project [12]. The code represents the turbulent, buoyantly-driven incompressible flow, heat transfer, mass transfer, combustion, soot, and absorption coefficient modelling aspects of the suite. Fuego is couple to another Sandia-developed code called Nalu for Participating Media Radiation (PMR) modelling, using Multiple-Program-Multiple-Data (MPMD) coupling.

Among the options for turbulence models in SIERRA Fuego, Large Eddy Simulation (LES) was used in this study, with closure obtained via the subgrid-scale (SGS) kinetic energy one-equation (or K SGS) closure model. The LES model resolves the behavior of the larger eddies explicitly, while modeling the small eddies characterized by the subgrid scale approximately. The difference between these divisions is characterized by length scale Δ, which, if the eddy size $\geq \Delta$, implies that the eddy belongs to the larger eddies that are resolved, and if the eddy is smaller than Δ, it belongs to the small eddy category which is modeled with subgrid-scale models [13,14]. LES was chosen to model the methanol pool fire analyzed in this study since it produces time-varying results. Having temporally-varying results was essential for calculation of statistics necessary for comparison with experimental data.

Methanol combustion was modeled using a Strained Laminar Flamelet Model (SLFM), in which the turbulent flames are treated as an ensemble of laminar diffusion flames, and nonequilibrium chemistry is included by accounting for localized fluid strain. By resolving chemical scales in the phase space of the mixture fraction instead of a three-dimensional grid, computational efficiency is improved [12]. In this model, chemistry is assumed to occur only in a thin layer around stoichiometry and to be quasi-steady on the scale of the flow. Thus, the chemical structure in mixture fraction space is pre-computed and tabulated, and the resulting table is queried during the simulation to obtain flow properties.

The simulated geometry imitated experimental setups for this validation case. Multiple features were geometrically important to the physics, including the pan diameter (30 cm), rim/lip height (1 cm), and distance of the pan above the floor (0.25 m from pool surface to floor). Pan elevation and lip height play an important role in the entrainment characteristics of the fire, and thereby affect dependent physics [15].

In Figure 1, the simulation domain and boundary conditions are shown. On the pool surface, mass flux was prescribed at 0.0151 kg/m^2-s, temperature was set to 333 K (boiling point of methanol), mixture fraction was specified as 1.0, and scalar variance was set to 0.0. A constant temperature (298 K) wall boundary condition was used at the bottom of the domain, and pan surfaces, and other domain boundaries were modeled as outflow-type boundaries, with the following conditions: gage pressure = 0, velocity = 0, mixture fraction = 0, temperature = 298 K. Other simulation parameters of interest may be found in Hubbard et al. [16].

The simulations were run with two grid refinement levels and the results examined to determine the effect of grid refinement on key quantities in the solution. The coarse mesh had 3,006,446 nodes and 2,363,433 cells, while the fine mesh had 6,177,500 nodes and 4,827,253 cells.

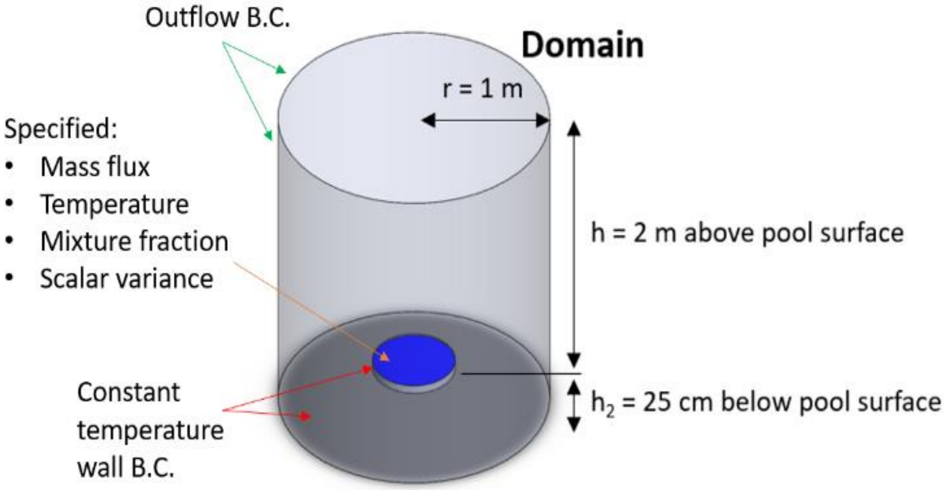

Figure 1: Simulation domain and boundary conditions.

3 THEORY

3.1 Area Validation Metric

Validation can be defined as the process of determining the degree to which a model is an accurate representation of the real world from the perspective of the intended uses of the model [17]. To perform a quantitative comparison between the results of the computational model and experimental results, various validation metrics can be applied. When data is obtainable as statistical distributions, comparisons may be drawn between distributions of experimental and simulation datasets. The area validation metric (AVM) is a metric which operates on such data, and has been employed by researchers such as Oberkampf and Roy [2, 17]. This metric is defined to be the area between the cumulative distribution function from the simulation and the empirical distribution function (EDF) which is also known as empirical cumulative distribution function from the experiment. In the case that the number of simulation samples is limited, the simulation may be represented by individual samples and an EDF for the simulation results may be used as well as for the experimental data. If the area between the EDF of the experiment and the EDF of simulation is 0, there is no evidence that results from the simulation and the experiment are in disagreement. The present study uses the AVM to analyze the time range necessary for accurate validation comparisons involving temporally-varying data from the simulation. The difference in areas under experimental and simulation distribution functions is designated as d. In the figures which present the AVM below, the colored areas are the difference between experimental and simulation cumulative values. The red area represents the positive difference (d^{+}) and the blue area represents the negative difference (d^{-}) which are evaluated for the model form uncertainty. If S is considered as the simulation mean value or the function simulation results, the model form uncertainty can be presented as $[S - F_s d^{-}, S + F_s d^{+}]$, $F_s = 1.25$, where F_s is the factor of safety [2, 17-19].

3.2 Radiative Heat Flux

Radiative heat flux is an important quantity in pool fires because significant heat is transferred to nearby or engulfed objects through radiative heat transfer. In addition, combustion temperature conditions near the pool surface are sustained in large part due to radiative heat feedback to the pool [20]. In the simulations used in the current study, the radiative heat transfer is computed as an integral of the scaled radiative intensity. The radiative intensity is solved for in the Boltzmann radiative transport equation.

4 RESULTS AND DISCUSSION

Three quantities are examined in this study: temperature, axial velocity, and radiative heat flux magnitude. Temperature is a key QOI for pool fires due to its relationship to combustion, buoyancy, and heat transfer. Axial velocity is important due to its critical role in momentum within the plume, convective heat transfer, and mass and species transfer. Radiative heat flux is important in sustaining the fire and transferring heat to the surroundings. Time-averaged temperature and axial velocity data were below experimental data over the spatial range considered, while the experimental trend crossed the computational trend for radiative heat flux magnitude.

The area validation metric is a useful metric in analyzing statistical datasets, and in the sections which follow, the importance of understanding such datasets and how the AVM should be applied is shown. The dataset examined in this study involves temporally-varying data from the LES simulations on the fine grid. Because flow within the plume fluctuates (indeed, a distinct puffing frequency arises and strongly influences flow quantities), taking a sufficiently long time interval for the computation of average quantities is critical. Use of insufficiently long time intervals could cause error and uncertainty estimates arising from the validation metric to be larger than they actually are, or serendipitously (and unrealistically) small.

4.1 Time-averaged QOIs

Contour plots of time-averaged temperature and axial velocity are shown in Figure 2. The temperature is the boiling point of methanol at the pool surface. There is a relatively high temperature core region which extends to roughly the average flame height, and temperature decreases radially from this region, and axially above and below. Axial velocity increases from zero at the pool surface to a maximum as buoyant affects and entrainment in eddies cause upward acceleration. Axial velocity decreases from the centerline radially. It is important to note that these plots are averaged over a long time range (10 s) to achieve representative behavior on a global temporal scale.

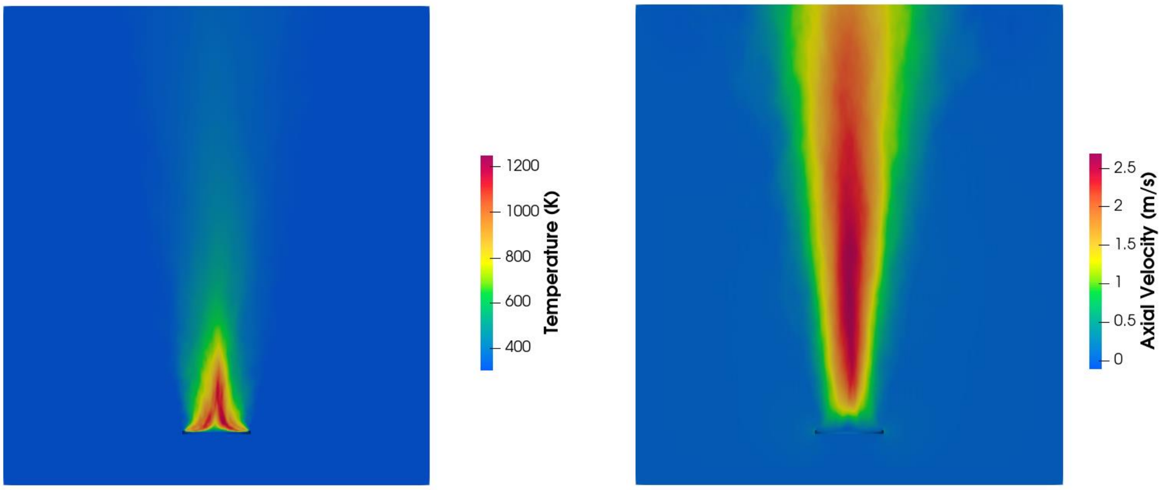

Figure 2: Contour plots of temperature and axial velocity.

In Figure 3, centerline trends from $z = 0$ to $z = 10$ cm are shown, for experimental data from Weckman [3] and simulation results on the coarse and fine meshes. All results show an increase in the QOIs over this spatial range and experimental results are everywhere higher than simulation results.

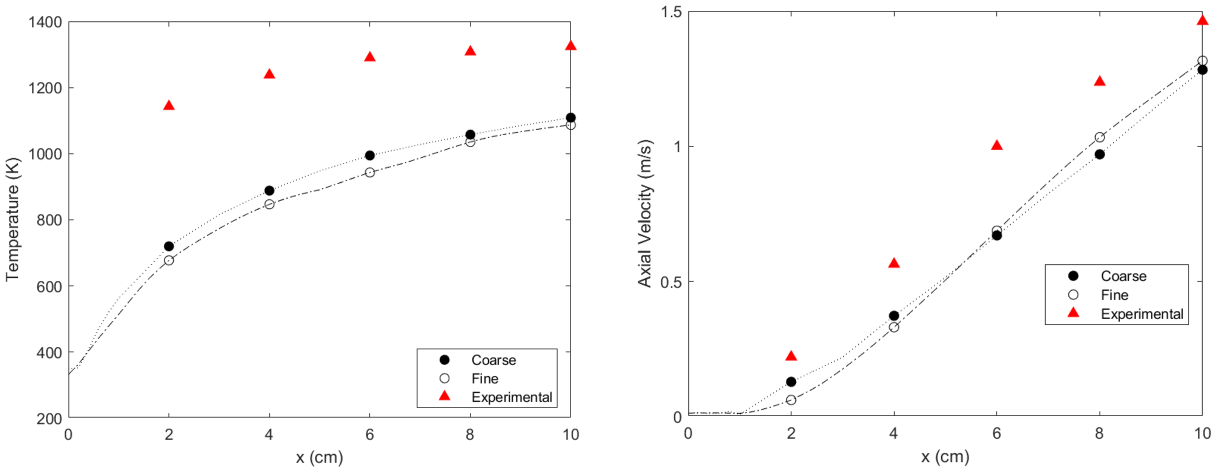

Figure 3: Axial trends of temperature and axial velocity along centerline.

A contour plot of radiative heat flux magnitude is shown in Figure 4 along with the radial trend of radiative heat flux magnitude (Q_{rad}). Just above the pool surface, Q_{rad} is high and decreases from the center of the pool, being directed downward in this region. The plot showing simulation and experimental datapoints is from this region, and shows that in general, Q_{rad} decreases radially. There is a cylindrical region of high Q_{rad} surrounding a core with relatively low values, and outside of the cylindrical region, Q_{rad} decreases radially and axially, as temperature decreases. The experimental data shown is from Hamins et al. [11].

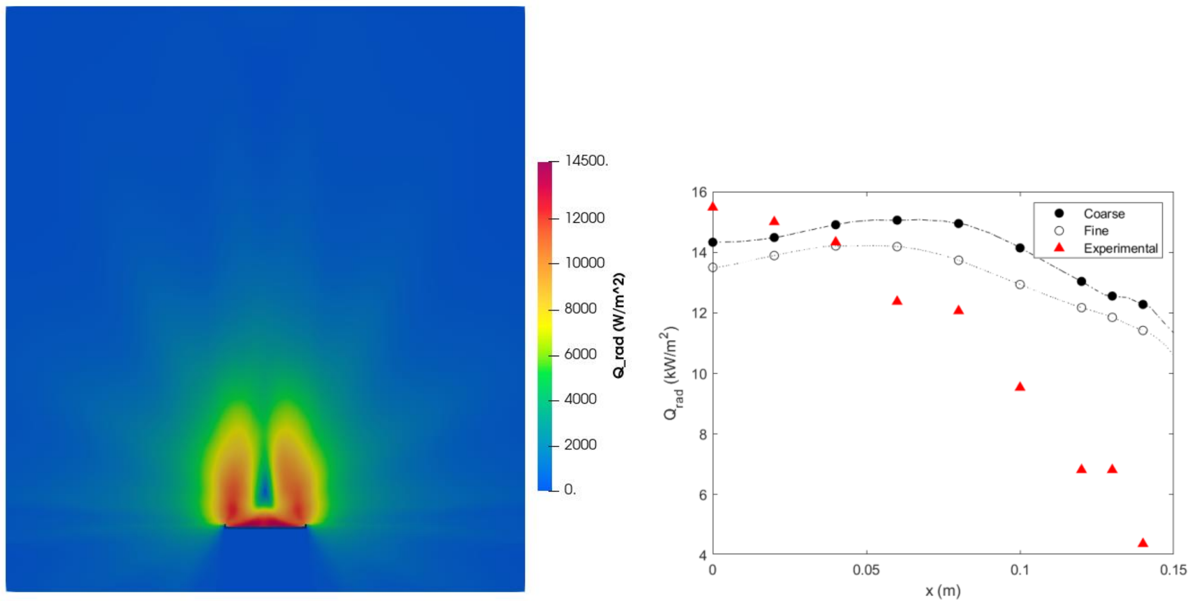

Figure 4: Contour plot of radiative heat flux magnitude (left) and radial distribution at z = 0.7 cm (right).

4.2 AVM Results, Temperature

In Figure 5, area validation metric plots for temperature are shown for four different time ranges at a spatial location of (x, y, z) = (0, 0, 0.04) m. Three plots are shown for 1 s time ranges, each spaced by 3 s from each other, and one plot is shown for a 10 s time range. The plot showing the time-series of data over 15-25 s is noticeably smoother than the other plots, and avoids the missing of the blue region (corresponding to d$^-$) in the plot with data from 20-21 s. Comparing the three 1 s plots, it can be observed that the distribution of temperature over time is different for each range and the probability that the temperature takes on a value above the time-averaged experimental value also varies between time series. The areas corresponding to when the simulation values are below (red) and above (blue) the experimental value are given in Table 1 as d$^+$ and d$^-$, respectively. Though the 23-24 s time range approximates the 10 s time range reasonably well, this cannot be depended on. In the worst case, the 20-21 s time range predicts zero uncertainty in the negative direction, and significantly overpredicts uncertainty in the positive direction.

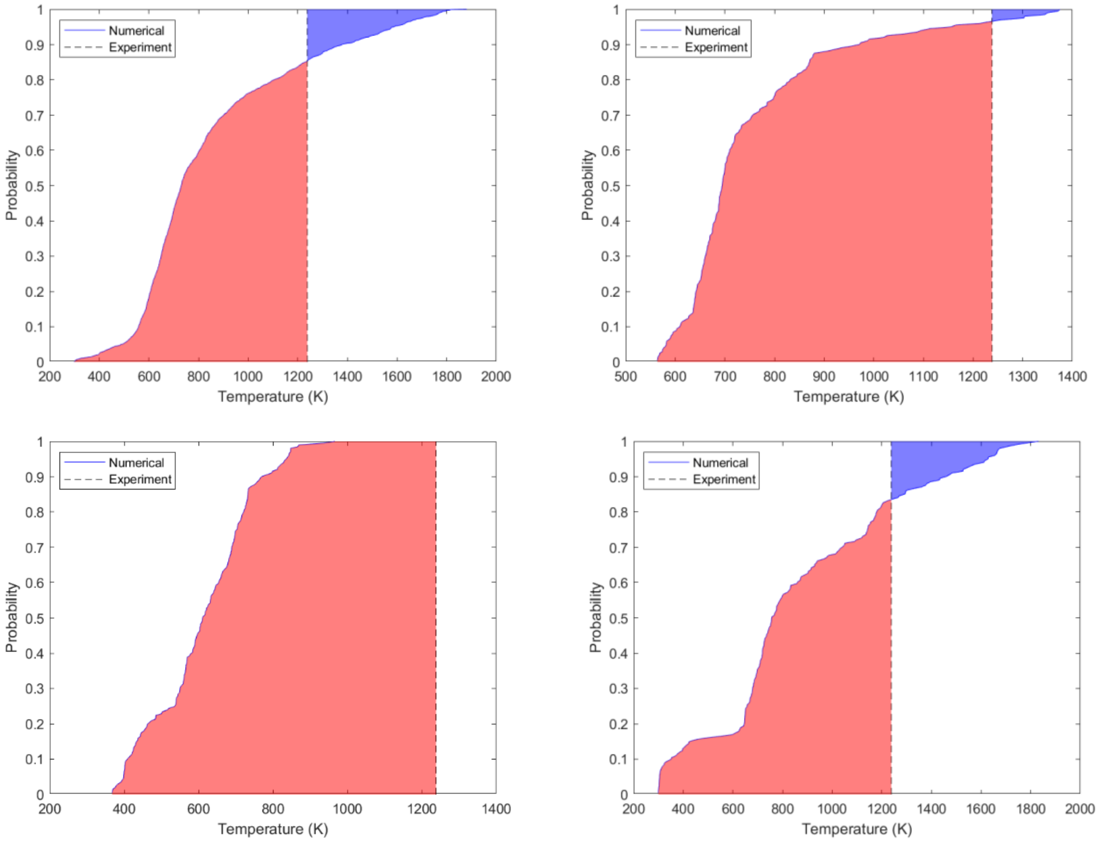

Figure 5: AVM plots for temperature at z = 4 cm, for 15-25 s (top left), 17-18 s (top right), 20-21 s (bottom left), 23-24 (bottom right).

Table 1: Difference areas from AVM for temperature.

QOI	d$^-$	d$^+$
T, 17-18 s	2.833	492.12
T, 20-21 s	0	628.73
T, 23-24 s	44.756	415.92
T, 15-25 s	38.888	428.96

4.3 AVM Results, Axial Velocity

AVM plots for axial velocity at the same spatial location as for temperature are given in Figure 6. Again, the 10 s time interval corresponds to the smoothest dataset, and shows balance of uncertainty between the right and left sides. The 1 s datasets only occasionally show the correct behaviour, both in terms of left/right behaviour and distribution shape. The result is that two of the datasets significantly underpredict negative uncertainty and overpredict positive uncertainty (Table 2).

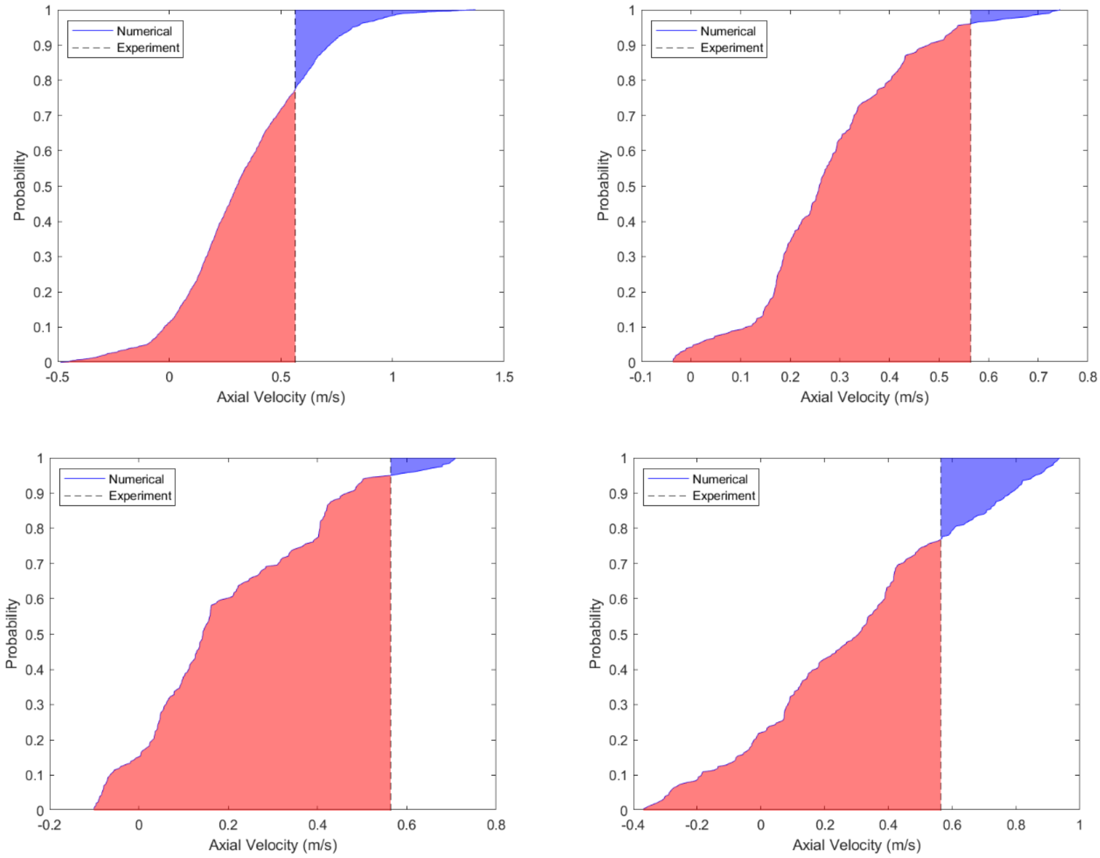

Figure 6: AVM plots for axial velocity at z = 4 cm, for 15-25 s (top left), 17-18 s (top right), 20-21 s (bottom left), 23-24 (bottom right).

Table 2: Difference areas from AVM for axial velocity.

QOI	**d^-**	**d^+**
U, 17-18 s	0.0039268	0.29386
U, 20-21 s	0.0047464	0.37528
U, 23-24 s	0.044283	0.32151
U, 15-25 s	0.039818	0.27332

4.4 AVM Results, Radiative Heat Flux Magnitude

AVM plots of radiative heat flux magnitude at (x, y, z) = (0, 0, 0.007) m are given in Figure 7. In these plots, the 1 s same time intervals are used as for temperature and axial velocity, and again, the 20-21 s time interval yields an overprediction of positive uncertainty, whereas the 20-23 s time interval is the most balanced of the 1 s time intervals. The fact that the general behavior of the QOI at each 1s time interval is similar points to the coupled physics involved in the fire and the fact that each QOI is influenced by the periodic nature of the flow.

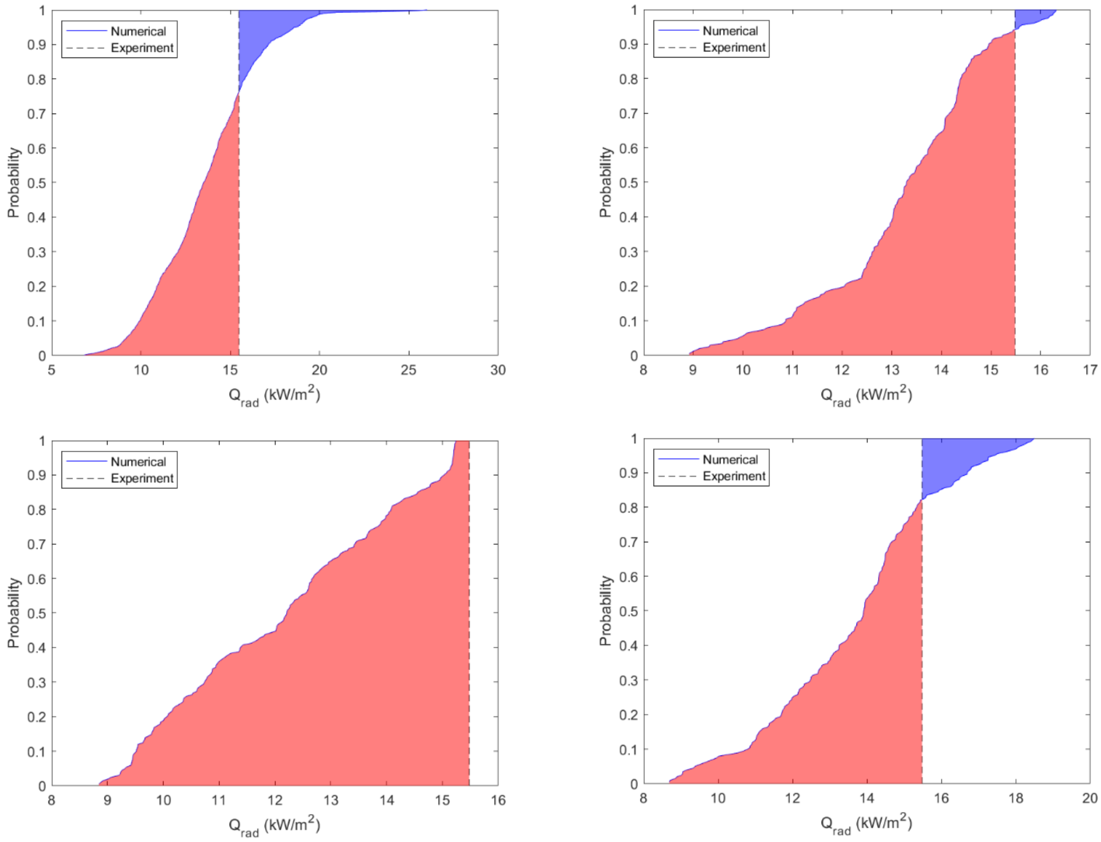

Figure 7: AVM plots for radiative heat flux at z = 4 cm, for 15-25 s (top left), 17-18 s (top right), 20-21 s (bottom left), 23-24 (bottom right).

Table 3: Difference areas from AVM for radiative heat flux.

QOI	**d^-**	**d^+**
Q_{rad}, 17-18 s	0.029201	2.3403
Q_{rad}, 20-21 s	0	3.3489
Q_{rad}, 23-24 s	0.25615	2.0974
Q_{rad}, 15-25 s	0.4466	2.3481

5 CONCLUSION

In this study, the area validation metric was used on three QOIs from a validation simulation using a Sandia National Laboratories code. Multiple time intervals were selected for the representative transient analysis, and the results showed that short time intervals were insufficient to capture average behavior for use with the validation metric. The flow's known periodic behavior, with a characteristic puffing frequency and differences from cycle to cycle demand the use of longer time intervals. The length of the time interval sufficient for representation of average behavior was found in a separate convergence study to be optimally 10 s, but as low as 5 s for some quantities. Such analysis is necessary to achieve useful quantitative results from the area validation metric on transient datasets.

REFERENCES

[1] Ferson, S., Oberkampf, W., Ginzburg, L., 2008, "Model validation and predictive capability for the thermal challenge problem", Computer Methods in Applied Mechanics and Engineering 197, pp. 2408 – 2430.

[2] Oberkampf, W. L., Roy, C. J., 2010, "Verification and Validation in Scientific Computing", Cambridge University Press.

[3] Weckman, E. J., Strong, A. B., 1996, "Experimental Investigation of the Turbulence Structure of Medium-Scale Methanol Pool Fires", Combust. Flame 105, pp. 245-266.

[4] Buch, R., Hamins, A., Konishi, K., Mattingly, D., Kashiwagi, T., 1997, "Radiative Emission Fraction of Pool Fires Burning Silicone Fluids", Combust. Flame 108, pp. 118-126.

[5] Falkenstein-Smith, R., Sung, K., Chen, J., Hamins, A., 2020, "Chemical Structure of Medium-Scale Liquid Pool Fires", Fire Safety Journal 120, 103099.

[6] Falkesntein-Smith, R., Sung, K., Chen, J., Harris, K., Hamins, A., 2020, "The Structure of Medium-Scale Pool Fires", NIST Technical Note 2082, National Institute of Standards and Technology.

[7] Hamins, A., Lock, A., 2016, "The Structure of a Moderate-Scale Methanol Pool Fire", NIST Technical Note 1928, National Institute of Standards and Technology.

[8] Kim, S.C., Lee, K.Y., Hamins, A., 2019, "Energy Balance in Medium-Scale Methanol, Ethanol, and Acetone Pool Fires", Fire Safety Journal 107, pp. 44-53.

[9] Klassen, M., Gore, J. P., 1994, "Structure and Radiation Properties of Pool Fires", NIST-GCR-94-651, National Institute of Standards and Technology.

[10] Wang, Z., Tam, W. C., Chen, J., Lee, K.Y., Hamins, A., 2019, "Thin Filament Pyrometry Field Measurements in a Medium-Scale Pool Fire", Fire Technology 56, pp. 837-861.

[11] Hamins, A., Fischer, S. J., Kashiwagi, T., Klassen, M. E., and Gore, J. P., 1994, "Heat Feedback to the Fuel Surface in Pool Fires," Combust. Sci. Technol., 97(1–3), pp. 37–62.

[12] Black, A., Aro, C., Brown, A., Burns, S., et al., 2021, "SIERRA Low Mach Module: Fuego Theory Manual – Version 5.0", Report No. SAND2021-3929, Sandia National Laboratories.

[13] Aleyasin, S. S., Fathi, N, Tachie, M. F., Peter Vorobieff, P., Koupriyanov, M., 2017, "Experimental-numerical analysis of turbulent incompressible isothermal jets", Fluids Engineering Division Summer Meeting, vol. 58066, p. V01CT23A015, American Society of Mechanical Engineers.

[14] Rodriguez, S. B., Fathi, N., "Applied Computational Fluid Dynamics and Turbulence Modeling", No. SAND2017-13577B. Sandia National Lab.(SNL-NM), Albuquerque, NM (United States), 2017.

[15] Ma, L., Nmira, F., Consalvi, J., "Large Eddy Simulation of medium-scale methanol pool fires - effects of pool boundary conditions", Combustion and Flame, 2020.

[16] Hubbard, J. A., Hansen, M. A., Kirsch, J. R., Hewson, J. C., Domino, S. P., 2022, "Medium Scale Methanol Pool Fire Model Validation", ASME Journal of Heat Transfer 144.

[17] Roy, C. J., Voyles, I., 2013, "Assessment of Model Validation Approaches using the Method of Manufactured Universes", ASME Verification and Validation Symposium.

[18] Shen, Yu-Lin, Fathi, N., 2022, "Numerical Study of Elastic-Plastic Behavior of Pore-Containing Materials: Effects of Pore Arrangement", International Journal of Theoretical and Applied Multiscale Mechanics, vol. 3, no. 4, pp. 262-286.

[19] Fathi, N., Aleyasin, S. S., Wayne, P, and Vorobieff. P., 2017, "Computational Assessment of Double-Inlet Collector in Solar Chimney Power Plant Systems", Fluids Engineering Division Summer Meeting, vol. 58059, p. V01BT08A006, American Society of Mechanical Engineers.

[20] Klassen, M., and Gore, J. P., 1994, Structure and Radiation Properties of Pool Fires, C. f. F. Research, ed., National Institutes of Standards and Technology, Gaithersburg, MD, pp. 1–156.